Spring Technical Meeting
Eastern States Section of the Combustion Institute
March 4-7, 2018
State College, Pennsylvania

Topology of Local Flame-Flame Interaction Events in Turbulent Flames

Ankit Tyagi[1], Isaac Boxx[2], Ryan Shupp[1], Stephen Peluso[1], and Jacqueline O'Connor[1,]*

[1]Mechanical and Nuclear Engineering, Pennsylvania State University, University Park, PA, USA
[2]DLR, German Aerospace Center, Stuttgart, Germany, 70596
[*]Corresponding Author Email: jxo22@psu.edu

Abstract: A large number of modern combustion devices have multiple, closely-spaced turbulent flames that interact with each other, resulting in interacting flowfields as well as scalar fields. The local structure and dynamics of adjacent flames is dependent on both these interacting fields. Local flame-flame interaction occurs frequently in turbulent flames, occasionally resulting in formation of unburned gas pockets, and in some cases, burned gas pockets. Unburned gas pockets can be a source of harmful pollutants, as they may result in toxic fuel emissions. The topology of interaction events can vary significantly in the presence of adjacent flames and it becomes crucial to understand the sensitivity of these flames to these local interaction events for improving the design and operability of multi-flame devices. In this study, we investigate two interacting premixed flames in a dual burner configuration and apply high-speed OH-planar laser-induced fluorescence (OH-PLIF) to obtain instantaneous flame-front locations of Bunsen flames. A non-rigid image registration technique is applied to flame images to track the topological changes occurring in small time steps. Flame-flame interaction events are identified using this technique and statistics conditioned on these events are compared. In particular, results are compared between single- and dual-burner configurations to illustrate the differences that interacting flames have on flame topology. Statistics of flame-flame interactions that result in flame pockets are also discussed.
Keywords: Turbulent flames, Flame-flame interactions

1. Introduction

Many modern combustion devices operate in multi-flame configurations and the interaction between adjacent flames in these devices can impact the flame shape, and the static and dynamic stability [1-5]. Flame-flame interactions affect the local structure and dynamics of turbulent flames and a detailed understanding of this local behavior is essential for predicting the global behavior of combustion devices. A number of studies have investigated flame-flame interactions [6-11] and results from these studies have shown that local flame-flame interactions can occur with either the consumption of reactant gases in between two flame-fronts (normal interactions), or the merging of the product sides of these flame-fronts (counter-normal interactions). Direct numerical simulations by Dunstan *et al.* [9, 10] and Griffiths *et al.* [6] have shown that the frequency of interactions vary with downstream distance and counter-normal interactions are more likely observed in shear layer regions with high strain rates and progress variables close to unity (towards products). Additionally, Chen *et al.* [12] have reported that flame wrinkling in turbulent flames leads to the beginning of interactions, such as a tunnel closure events, which lead to flame cusps and pocket formation. Results from their study have shown that these effects correspond to a sharp decrease in the local flame area, flame stretch, and the volumetric heat release. Global stretch rates calculated by Dunstan *et al.*[9, 10] also show bias to negative values and these rapid fluctuations in flame

area and flame stretch from flame interactions also affect the flame speed. Chen *et al.*[12] have shown that the density-weighted displacement speed can increase by a factor of four during a pocket burnout event. These previous DNS studies have provided a detailed understanding of individual interaction events occurring in turbulent flames. However, analyzing flame-flame interactions for parametric variation of operating conditions becomes computationally expensive and experiments seem a viable approach towards obtaining statistical information for such dynamic events in turbulent flames. The goal of this study is to document the effect of adjacent flames on local flame-flame interaction events by providing statistical information of the characteristics of these events.

2. Methods / Experimental

2.1 Burner Configurations and Diagnostics

Measurements are performed in a dual slot-burner experimental facility, where the slot burners are mirror images along the experiment centerline (Figure 1). Stoichiometric premixed mixtures of fuel (natural gas) and air at room temperature enters the lower section of each burner and passes through two layers of ceramic honeycombs for flow conditioning. Two perforated plates placed at 30 mm and 10 mm upstream of the burner exit plane are used to create averaged turbulence intensities of 18% in the flowfield. The exit plane for each burner is 100 mm x 10 mm and this large-aspect ratio allows for obtaining time-averaged two-dimensional flowfields in our experiments. Each burner is equipped with two types of pilot flames, operated at stoichiometric conditions, along the 100 mm side of the slot: small 'anchoring' pilots, which are located close to the exit of the burners and help stabilize atmospheric pressure flames on the experiment, and larger 'back-support' pilots, which provide adiabatic or super-adiabatic combustion products around the flames. The burners are mounted to a small mill stage, which allows for changing fields-of-views (FOVs) for laser measurements. Conversion to single burner configuration involves attaching the back-support pilot flames of the right burner as a secondary pilot to the left burner to make the flow configuration symmetric on the left burner. High-speed flame-front measurements are performed using OH-planar laser-induced fluorescence (OH-PLIF) at a sampling rate of 10 kHz. The OH-PLIF system consists of a 532 nm Nd:YAG laser (Edgewave) pumping a dye laser (Sirah Credo). The output beam is calibrated to the $Q_1(6)$ line of the $A^2\Sigma^+ \leftarrow X^2\Pi$ (1-0) band to excite the OH radicals at 282.94 nm. The UV beam from the dye laser is passed through a periscope and a set of three cylindrical lenses to obtain a collimated sheet with an approximate height of 21 mm. The signal from the excited OH radicals is acquired using a CMOS sensor camera (Photron FASTCAM SA1.1), coupled with an external intensifier (LaVision HS-IRO) and a 100 mm f/2.8 UV lens (Cerco), resulting in a resolution of 0.1 mm/pixel. Measurements are performed in three FOVs with a 5mm overlap between two FOVs and FOV I begins at 5 mm downstream of the burner exit plane. Additional details of the experiment and laser diagnostics are provided in Ref. [13].

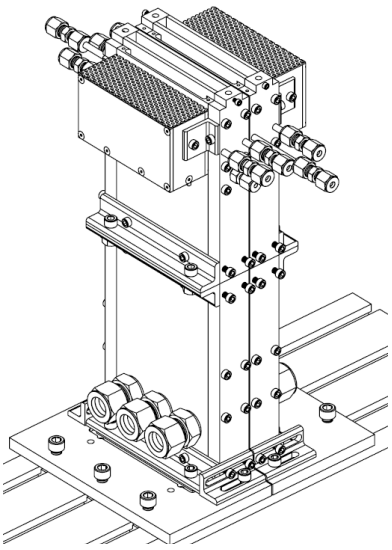

Figure 1: Schematic of the dual slot-burner experiment

2.2 Data Analysis Techniques

To obtain binarized images for edge-detection, raw OH-PLIF images are corrected for laser sheet intensity variations, and are median and bilateral filtered to reduce noise levels. Otsu's method is utilized for dynamic thresholding to obtain binarized images. Flame edges are obtained by tracing the edges of the binarized images using the '*bwboundaries*' function in MATLAB. Flame curvature of the traced flame edges is calculated by smoothing edges using the Savitzky-Golay filter, which uses a third order polynomial fit for sets of 15 pixels, along the entire flame edge. First and second partial derivatives of the smooth edge are calculated based on numerical approximations and are used to calculate the curvature of the flame edge. A non-rigid image registration technique (described as Automatic Feature Extraction in [9, 10]) is utilized

to identify local flame-flame interaction events. In this technique, translation operations are performed on consecutive image pairs to account for local convection in the flowfield and resulting differences are recorded, which correspond to topological differences in these flames within 100 μs.

3. Results and Discussion

Figure 2 shows the stitched flame surface density images of the Bunsen-stabilized flames operating at a bulk flow velocity of 12 m/s and ϕ=1.0 in the dual- and single flame configurations. For the dual flame case, the inner side walls of the burners are adjacent, creating a center-to-center distance of 30 mm between the burner centerlines. Flame surface density is calculated by identifying instantaneous flame edges in a small interrogation region and averaging the results over 9999 frames. The single flame case is shown here as a reference for flame structure obtained at this flow velocity in our experiments. As shown in Figure 2, the global effect of interacting flames is particularly pronounced in FOVs II and III; the presence of adjacent flames in the dual-flame case changes the time-averaged flame structure by affecting the inner flame branches in these flames, as they are subjected to different boundary conditions. To compare the local structure of these flames, curvatures for each flame are calculated as outlined in Section 2.2. Figure 3 shows the probability density functions (PDFs) of flame curvatures in FOVs I, II, and III for the single- and dual flame cases. For the rest of the paper, 'Dual-left' corresponds to the left flame and 'Dual-right' corresponds to the right flame in the dual flame case. PDF trends of all flames in all FOVs show a good general agreement between each other; in general, the trends are distributed about zero, indicating similar amounts of wrinkling in these flames. While these curvature PDFs report the statistics of the local topology of these flames and provide us with information on the wrinkling of these flames, it is challenging to obtain any information on the dynamically changing topology of these flames.

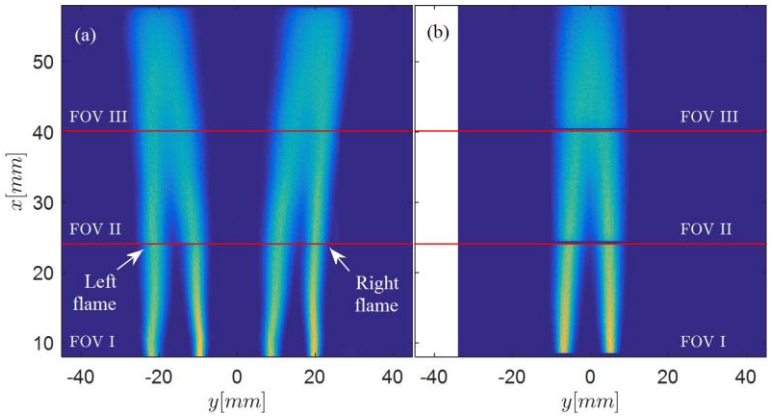

Figure 2: Stitched flame surface density image of Bunsen flames at U=12 m/s, ϕ=1.0 in the (a) dual flame, and (b) single flame configurations

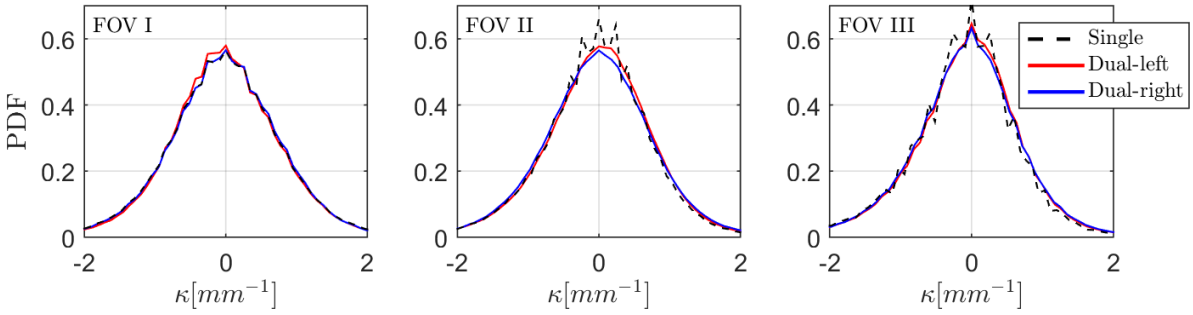

Figure 3: PDF of flame curvatures for the single flame and dual flame cases

The application of the non-rigid image registration technique permits identification and tracking of topological differences existing between two image pairs. Figure 4 shows a time-series of the flame-flame interaction events occurring in the left burner flame in FOV I where topological differences are highlighted in white closed contours. As shown with arrows in the figure, different types of flame-flame interactions can occur in turbulent flames: flame-front merging leading to pocket formations, merging of existing pockets in attached flame-fronts, breaking of pockets into several smaller pockets, etc. Flame tips are occasionally observed for these flames in FOV II (not shown here), where big flame pockets are formed that propagate into FOV III and either break into smaller pockets or get consumed further downstream.

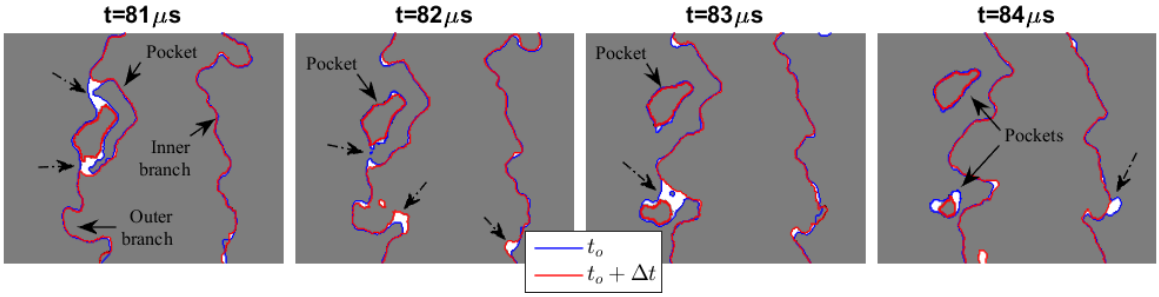

Figure 4: Time-series of flame-flame interactions for left burner flame in FOV I

All identified interactions over a range of 9998 images are reported in Figure 5(a). The total number of interaction events occurring in FOV I are very similar for both single and dual flames; however, these numbers vary significantly in FOV II and III. These trends indicate that near the flame attachment region, the dynamics of flames are similar for both single- and dual-burner cases. The presence of adjacent flames starts to affect the flames in FOVs II and III. To isolate the influence of flame pockets on attached flame-fronts and merging/breaking of flame pockets, pocket interactions are filtered out so that only interactions occurring along the main attached flame are counted. These filtered interactions are presented in Figure 5(b); the number of filtered interactions decrease for all flames as a function of FOV. FOVs II and III correspond to the flame tip region and a high frequency of formation of big flame pockets exist in these FOVs. Differences in the pocket-filtered interaction counts in FOVs II and III show that a large number of flame-flame interactions occur in the attached flame fronts in the dual flame case, which are lower for the single flame case. A high number of total flame interactions and a low number of filtered flame interactions in FOV II for the single flame case suggests that in this region, a high frequency of interactions is attributed to existing flame pockets that interact with the attached flame fronts or other existing pockets.

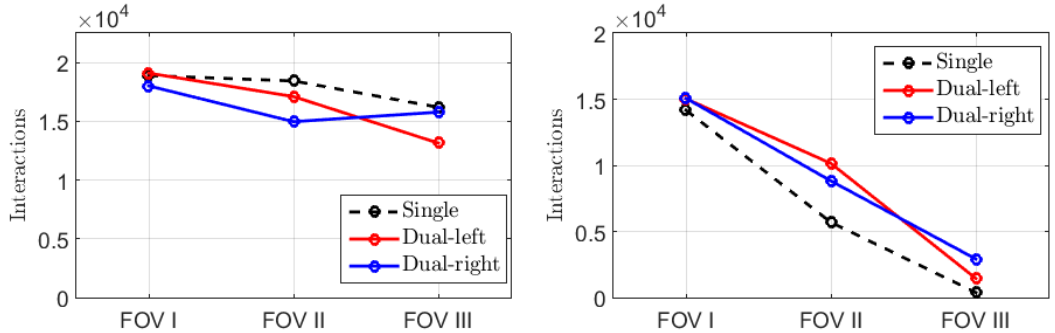

Figure 5: (a) Total number of flame interaction numbers, (b) filtered flame-flame interaction numbers

Centroids of the interaction zones, shown as white closed contours in Figure 4, correspond to a representative location of instantaneous, filtered flame-flame interactions and statistics conditioned on these centroids are presented in Figure 6. A comparison of PDF trends of filtered interaction conditioned averaged progress variables ($\bar{c}$) (shown in Figure 6(a)) show similarities between the left and right flames for the dual flame case, however, slight deviations can be seen for the single flame case. For all FOVs, a higher probability exists for interactions occurring at locations of $\bar{c} > 0.5$ of the flame brush. These results are congruent with results of Griffiths *et al.* [6] and Dunstan *et al.* [9, 10] that have reported high frequencies of interactions occurring along the leading and trailing edges of the flame brush. For FOV III, the PDF peaks close to $\bar{c} \approx 0.9$ for the single flame case, whereas, for the dual flame, this peaks is closer to $\bar{c} \approx 0.75$. PDFs of filtered interaction conditioned curvatures for all flames are shown in Figure 6(b). The PDF distributions for all FOVs shown in this figure are centered close to zero, which indicates that a normal-type distribution of interaction conditioned curvatures are present in all FOVs. Dunstan *et al.* [9, 10] have reported that for normal interactions, positive principal curvatures correspond to convex-normal interactions and negative principal curvatures correspond to tunnel-closure and pocket burn out interactions. The curvature distributions suggest that these types of interactions are present in all FOVs for the flames investigated here.

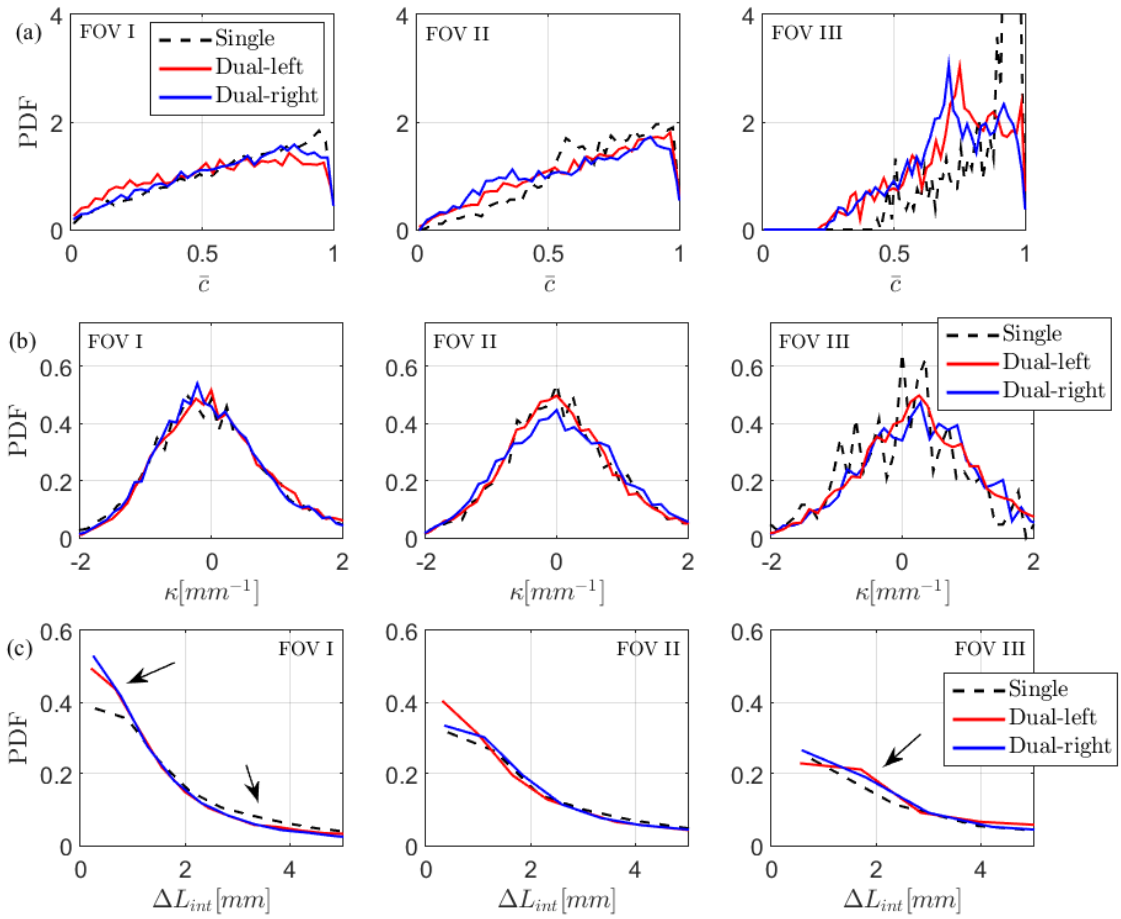

Figure 6: PDF of filtered flame-flame interaction conditioned (a) averaged progress variables ($\bar{c}$), (b) flame curvatures (κ), and (c) flame length scale differences before and after interactions (ΔL_{int})

Differences in the length scales due to flame-flame interactions are also extracted and probabilities of these length scales are presented in Figure 6(c). A close look at the PDFs of these length scales in FOV I shows higher probabilities of small length scales for the dual flame case, as compared with the single flame case. These differences are small for these flames in FOVs II and III. This is an important finding and will require further investigation of the velocity fields to understand the differences in the turbulence fields of these flames. Table 1 shows the number of pocket formations due to filtered flame-flame interactions in FOVs I and II for the single- and dual flame cases. Smaller differences exist for these flame in FOV I, however, these differences become large in FOV II. This is likely due to the differences in the averaged location of flame tip in the single- vs. dual flame case. These results indicate that the presence of adjacent flames can change the dynamics of flame-flame interactions in turbulent premixed flames.

Table 1:Number of filtered interactions leading to pocket formations for 9998 images

	FOV I	***FOV II***
Single	***1756***	***747***
Dual-left	***1596***	***1371***
Dual-right	***1479***	***1250***

4. Conclusions

High-speed OH-PLIF is implemented to study the effect of interacting flames on the local topology of flame fronts and statistics conditioned on local flame-front reduction events are presented. Instantaneous movies of these flames reveal that the local dynamics of flame-fronts can vary with the presence of adjacent flames and it is challenging to interpret this using flame-front curvature statistics. With the aid of image registration methodologies, dynamics of flame-flame interactions are tracked to capture these broad-range

scale interactions. Higher probabilities of small length scales associated with flame-flame interactions in the branches of these flames indicate short times associated with consumption of these flame-front elements. Unburned gas pocket formation is a dominating phenomenon occurring further downstream of the attachment region and larger pockets are formed near the flame tip region. These larger flame pockets break into several smaller pockets and get consumed further downstream. Future work from this experiment will include dynamic tracking of flame pockets and capturing their consumption rates. These analysis techniques will be implemented to a large data set to study the effects of parametric variation in the current burner configuration. Instantaneous velocity fields will also be analyzed to support these findings.

5. Acknowledgements

This work was supported by the Air Force Office of Scientific Research under Grant FA9550-16-1-0075 with program manager Dr. Chiping Li. The authors would also like to thank the students of the Reacting Flow Dynamics Lab for their support.

6. References

1. Worth, N.A. and J.R. Dawson, *Tomographic reconstruction of OH* chemiluminescence in two interacting turbulent flames.* Measurement Science and Technology, 2012. **24**(2): p. 024013.
2. Samarasinghe, J., et al., *Three-Dimensional Chemiluminescence Imaging of Unforced and Forced Swirl-Stabilized Flames in a Lean Premixed Multi-Nozzle Can Combustor.* Journal of Engineering for Gas Turbines and Power, 2013. **135**(10): p. 101503.
3. Hegde, U., et al., *Flame driving of longitudinal instabilities in dump type ramjet combustors.* Combustion Science and Technology, 1987. **55**(4-6): p. 125-138.
4. Dawson, J.R. and N.A. Worth, *Flame dynamics and unsteady heat release rate of self-excited azimuthal modes in an annular combustor.* Combustion and Flame, 2014. **161**(10): p. 2565-2578.
5. Aguilar, M., et al., *Helical Flow Disturbances in a Multinozzle Combustor.* Journal of Engineering for Gas Turbines and Power, 2015. **137**(9): p. 091507.
6. Griffiths, R., et al., *Three-dimensional topology of turbulent premixed flame interaction.* Proceedings of the Combustion Institute, 2015. **35**(2): p. 1341-1348.
7. Sohrab, S., Z. Ye, and C. Law. *An experimental investigation on flame interaction and the existence of negative flame speeds*. in *Symposium (International) on Combustion*. 1985. Elsevier.
8. Chung, S., J. Kim, and C. Law. *Extinction of interacting premixed flames: theory and experimental comparisons*. in *Symposium (International) on Combustion*. 1988. Elsevier.
9. Dunstan, T., et al., *Flame interactions in turbulent premixed twin V-flames.* Combustion Science and Technology, 2013. **185**(1): p. 134-159.
10. Dunstan, T., et al., *The effects of non-unity Lewis numbers on turbulent premixed flame interactions in a twin V-flame configuration.* Combustion Science and Technology, 2013. **185**(6): p. 874-897.
11. Im, H.G. and J.H. Chen, *Preferential diffusion effects on the burning rate of interacting turbulent premixed hydrogen-air flames.* Combustion and flame, 2002. **131**(3): p. 246-258.
12. Chen, J.H., T. Echekki, and W. Kollmann, *The mechanism of two-dimensional pocket formation in lean premixed methane-air flames with implications to turbulent combustion.* Combustion and flame, 1999. **116**(1): p. 15-48.
13. Tyagi, A., et al. *Structure of Flames in Flame Interaction Zones*. in *2018 AIAA Aerospace Sciences Meeting*. 2018.